Aerosol Science and Technology, 38:938–947, 2004

ISSN: 0278-6826 print / 1521-7388 online
DOI: 10.1080/027868290511236

A Model of Deposition of Hygroscopic Particles in the Human Lung

B. Asgharian
CIIT Centers for Health Research, Research Triangle Park, North Carolina

Many aerosols in the environment are hygroscopic and grow in size once inhaled into the humid respiratory tract. The deposited amount and the distribution of the deposited particles among airways differ from insoluble particles of the same initial diameter. As particles grow in size, diffusive behavior tends to diminish while impaction and sedimentation effects increase. A multiple-path model for deposition of hygroscopic particles in the respiratory tract was developed for symmetric and asymmetric lung geometries by implementing particle size change in a model of insoluble particle deposition in lungs. Particle growth by molecular diffusion of water vapor to the particle surface was formulated. The growth model included temperature depression, solute, Kelvin, and Fuchs effects. Particle growth during travel time in each lung airway was computed. Average loss efficiency per airway was calculated by incorporating contributions from particles of various sizes acquired in that airway. A mass balance on the number of particles that entered, exited, deposited, or remained suspended was performed per airway to obtain regional and local deposition fractions of particles in the lung. The deposition fractions calculated for salt particles showed a drop for submicrometer particles in the tracheobronchial region and a significant increase in deposition for micrometer particles or larger. Consequently, very few fine and coarse salt particles reached the alveolar region to be available for deposition. Overall, lung deposition of ultrafine particles decreased for salt particles. Deposition for fine and coarse salt particles in the lung was larger than that of insoluble particles of the same initial particle size.

INTRODUCTION

Many pollutants in the environment contain water-soluble species that will absorb water vapor and grow in size when inhaled into the respiratory tract (USEPA 1996; Spurny 1996; Lippmann and Thurston 1996). Inhalation of these particles may lead to lung injury, particularly in susceptible subpopulations such as children and the elderly (Spengler et al. 1990; Thurston et al. 1994). In addition, there are numerous hygroscopic pharmaceutical aerosols formulated for targeted delivery to the respiratory system. Deposition of insoluble particles in the extrathoracic region or first few airway generations of the lung may be similar to that of hygroscopic particles with the same initial diameter as that of insoluble ones, but it is quite different in the deep lung.

Treatment of hygroscopic particle deposition in models of the respiratory tract is markedly different from that of insoluble particles, since hygroscopic particles may undergo continuous size change during travel in the lung; an increase in size directly influences the amount and site of deposition (Martonen 1982; Xu and Yu 1985; Persons et al. 1987; Stapleton et al. 1994). The approach to finding deposition of insoluble particles is rather straightforward. Given the lung structure and airway dimensions along with the airflow field in different airways, deposition fraction in a given site or region within the lung is calculated from a mass balance on aerosols traveling in the region of interest. The aerosol mass balance incorporates deposition efficiency formulae for different loss mechanisms for that region. For insoluble particles and steady-state breathing, processes are time independent and can be solved uniquely for the entire breathing cycle (Yu 1978; Anjilvel and Asgharian 1995). However, hygroscopic particles may grow continuously during a breathing cycle, making the transport processes time-dependent. As a result, the unsteady Eulerian equations of particle transport have to be solved at each time point during a breathing period. Thus, calculations of hygroscopic particle deposition are more complex than those for insoluble particles.

Particle growth in the lung is largely influenced by the temperature and relative humidity throughout the lung. These quantities have not been directly measured in the lung, making deposition modeling somewhat hypothetical. A number of deposition models of hygroscopic particles in the lung have been developed (Martonen 1982; Persons et al. 1987; Ferron et al. 1988b; Martonen and Zhang 1993; Robinson and Yu 1998; Broday and Georgopoulos 2001). Existing models mainly use typical-path

Received 4 March 2004; accepted 9 July 2004.
This study was supported by Long Range Research Initiative of the American Chemistry Council. The authors are grateful to Dr. Barbara Kuyper for her editorial review.
Address correspondence to B. Asgharian, CIIT Centers for Health Research, Six Davis Drive, P.O. Box 12137, Research Triangle Park, NC 27709-2137, USA. E-mail: asgharian@ciit.org

symmetric lung structures that are not capable of fully capturing the effect of lung structural heterogeneity coupled with nonlinear growth of particles. While adoption of symmetric geometry may be justified for regional calculations of insoluble particles, its use for growing particles may introduce additional uncertainties since particle growth along short and long pathways may be underestimated or overestimated. Thus, a significant difference in particle deposition may occur for symmetric and asymmetric lung geometries. The deposition results calculated in symmetric and asymmetric lung geometries will differ in direct proportion to the degree of heterogeneity of the lung structure. The growth and deposition of particles in the human lung was studied in this article. A hygroscopic particle growth model was incorporated into an existing model of particle deposition in a multiple-path lung geometry for insoluble particles (Anjilvel and Asgharian 1995) to obtain a deposition model for hygroscopic particles. Using the model, deposition of hygroscopic particles in various regions of the lung was calculated and compared with that for insoluble particles.

MODELING APPROACH

Particle Growth Model

Hygroscopic particles grow in humid environments by condensation of water vapor on the surface of the particles. The growth rate for airborne particles depends on particle initial diameter, temperature, and relative humidity. The expression describing the growth of a particle of diameter d_p is given by Hinds (1999) as

$$\frac{dd_p}{dt} = \frac{M_w}{\rho_w \bar{R}} \frac{4D_w}{d_p}\left(\frac{P_\infty}{T_\infty} - \frac{P_d}{T_d}\right), \qquad [1]$$

where M_w, ρ_w, and D_w designate molecular weight, mass density, and diffusion coefficient, respectively, of water vapor; $\bar{R}$ is the universal gas constant; and P and T are partial pressure and temperature at the surface of the particle (denoted by subscript d) and away from it in the undisturbed environment (denoted by subscript ∞). Particle growth is determined solely by absorption of water vapor. The droplet is composed of solute (initial particle) and solvent (water vapor) components.

Partial pressure of water vapor is referred to as *equilibrium vapor pressure* when equilibrium conditions between the liquid and vapor phases are achieved. At the liquid–vapor interface for a flat plate, the equilibrium vapor pressure equals saturation vapor pressure, which is the pressure of the saturated vapor at the surface temperature of the liquid. For droplets, the equilibrium vapor pressure just above the droplet is higher than the saturation vapor pressure because the curvature of the droplet surface allows water molecules to leave the surface more easily. Thus, a higher vapor pressure is required to maintain equilibrium. The equilibrium vapor pressure of water vapor in the vicinity of the particle is related to the saturation vapor pressure via the Kelvin relationship (Hinds 1999) given by the equation

$$P_{d'} = P_s|_{T_d} \cdot e^{\frac{4\sigma M_w}{d_p \rho_w R T_d}}, \qquad [2]$$

where $P_s|_{T_d}$ is the saturation vapor pressure of the solvent (water vapor) at the droplet temperature, T_d, σ is the surface tension for water vapor, and $P_{d'}$ refers to equilibrium vapor pressure just above the droplet when only the Kelvin effect is present.

If the droplet contained only water vapor, Equation (2) could be used in Equation (1) to find particle growth. However, the presence of the solute in the droplet reduces the equilibrium vapor pressure since fewer molecules of water vapor are available on the surface of the droplet for transfer into vapor phase. The relationship between equilibrium vapor pressure of a droplet containing impurities and that of a droplet of pure water vapor is given by Friedlander (1977):

$$P_d|_{T_d} = \gamma \cdot x \cdot P_{d'}|_{T_d}, \qquad [3]$$

where γ is the activity coefficient and x the mole fraction of water vapor. In addition, the mole fraction of water vapor can be shown to be (Robinson and Yu 1998)

$$x = \left(1 + \frac{\frac{m_0}{M_s}\frac{M_w}{\rho_w}}{\frac{\pi d_p^3}{6} - \frac{m_0}{\rho_s}}\right)^{-1}, \qquad [4]$$

where M_s, ρ_s, and m_0 are the molecular weight, mass density, and mass of the solute (initial particle), respectively. By substituting Equation (4) into Equation (3), and then the result into Equation (2) and then into Equation (1), and expressing partial pressure in the undisturbed environment in terms of saturation vapor pressure, the following equation is obtained:

$$\frac{dd_p}{dt} = \frac{4D_w M_w}{\rho_w \bar{R} d_p}\left(\frac{P_{s0}|_{T_\infty}}{T_\infty} S - \frac{\gamma P_s|_{T_d}}{T_d} \times \left(1 + \frac{\frac{m_0}{M_s}\frac{M_w}{\rho_w}}{\pi d_p^3/6 - \frac{m_0}{\rho_s}}\right)^{-1} e^{\frac{4\sigma M_w}{d_p \rho_w R T_d}}\right), \qquad [5]$$

where S is the saturation ratio. For ultrafine particles, particle size approaches the mean-free path of air, and Equation (5) has to be corrected for the Fuchs effect to be valid in the slip and free molecular regimes (Davies 1978):

$$\frac{dd_p}{dt} = \frac{4D_w M_w}{\rho_w \bar{R} d_p} \times \frac{Kn + 1}{1 + 1.3325Kn^2 + 1.71Kn}\left(\frac{P_{s0}|_{T_\infty}}{T_\infty} S - \frac{\gamma P_s|_{T_d}}{T_d}\left(1 + \frac{\frac{m_0}{M_s}\frac{M_w}{\rho_w}}{\pi d_p^3/6 - \frac{m_0}{\rho_s}}\right)^{-1} e^{\frac{4\sigma M_w}{d_p \rho_w R T_d}}\right), \qquad [6]$$

where $Kn = 2\lambda/d_p$ is the Knudsen number and λ is the mean free path of air. The saturation vapor pressure at the droplet surface temperature is related to the saturation vapor pressure at

the temperature of the surrounding environment by the Clausius-Clapeyron relationship (Van Wylen and Sonntag 1973):

$$P_s|_{T_d} = P_s|_{T_\infty} \cdot e^{\left[\frac{h_{fg}M_w}{R}\left(\frac{1}{T_\infty}-\frac{1}{T_d}\right)\right]}, \quad [7]$$

where h_{fg} is the latent heat of condensation. Substituting Equation (7) into Equation (6) yields

$$\frac{dd_p}{dt} = \frac{4D_wM_wP_{s0}|_{T_\infty}}{\rho_w\bar{R}d_p} \times \frac{Kn+1}{1+1.3325Kn^2+1.71Kn} \times \left[\frac{S}{T_\infty} - \gamma\left(1+\frac{\frac{m_0}{M_s}\frac{M_w}{\rho_w}}{\pi d_p^3/6-\frac{m_0}{\rho_s}}\right)^{-1} \times \frac{e^{\frac{4\sigma M_w}{d_p\rho_w\bar{R}T_d}+\left[\frac{h_{fg}M_w}{R}\left(\frac{1}{T_\infty}-\frac{1}{T_d}\right)\right]}}{T_d}\right]. \quad [8]$$

When the droplet temperature is different from the surrounding temperature, the particle undergoes rapid temperature change to reach thermodynamic equilibrium. Consequently, the size change cannot be described solely by Equation (8). An additional expression describing the evolution of droplet surface temperature as a function of relative humidity and time such as that proposed by Broday and Georgopoulos (2001) becomes mandatory. For slow-growing particles, however, the droplet temperature approaches that in the environment very rapidly. Equation (8) further reduces to

$$\frac{dd_p}{dt} = \frac{4D_wM_wP_s|_{T_\infty}}{\rho_w\bar{R}d_pT_\infty} \times \frac{Kn+1}{1+1.3325Kn^2+1.71Kn} \times \left(S-\gamma\left(1+\frac{\frac{m_0}{M_s}\frac{M_w}{\rho_w}}{\pi d_p^3/6-\frac{m_0}{\rho_s}}\right)^{-1} e^{\frac{4\sigma M_w}{d_p\rho_w\bar{R}T_\infty}}\right), \quad [9]$$

indicating that the droplet has attained the surrounding temperature before the occurrence of any particle growth. Ultrafine and fine particles grow rapidly in the humid environment, and thus the use of Equation (9) is technically not justified. However, ultrafine particles reach their final size very rapidly while in extrathoracic airways and can essentially be treated as insoluble particles of a size larger than their initial size when entering the lung. In fact, particles smaller than 1 μm have little if any growth in the airway (see Figure 4). Overall, the error introduced by the use of Equation (9) is within the variability of the deposition models and should not affect the final deposition results. Equation (9) resembles other theoretically derived expressions such as those of Robinson and Yu (1998) and Broday and Georgopoulos (2001) if the effects of solute impurities and temperature difference between the droplet surface and surrounding are accounted for.

For the case of dilute, nonreacting droplets, $\gamma = 1$. Given the initial mass, molecular weight, and mass density, growth of particles of different initial compositions can be predicted from Equation (9). This equation can be safely used to describe growth of hygroscopic particles in the lung since inhaled particles are quickly reconditioned in the extrathoracic region and are near body temperature when entering the lower respiratory tract.

Mathematical Model of Particle Deposition

The deposition model used to calculate particle losses in the lung is a variation of an earlier model of Anjilvel and Asgharian (1995) that allows for particle growth during aerosol transport in the lung. Various assumptions are made in this model to facilitate the calculation of particle deposition fractions. The airflow velocity at a location within an airway is assumed uniform and proportional to the lung volume distal to that location. Consequently, the airflow rates decrease distally in an airway and within the lung. At the same time, lung airways expand and contract linearly during a breathing cycle that includes inhalation, pause, and exhalation. Deposition calculations are performed at a lung volume at midpoint between the lung at rest (functional residual capacity or FRC) and maximum inhalation. Axial diffusion and dispersion of particles have also been neglected. Particles are also assumed to be monodisperse and uniformly distributed in the tidal air. Particle loss at an airway occurs by sedimentation, impaction, and diffusion.

A mathematical model of particle deposition in an asymmetric lung geometry described elsewhere (Anjilvel and Asgharian 1995) is used to calculate particle deposition in various regions of the lung. The deposition model calculates deposition fractions of particles at various locations in the respiratory tract during a single breathing cycle in several steps. First, the airflow velocities in all airways of the lung are calculated. Second, the aerosol transport and distribution in the tidal air across lung airways are accounted for during a single breath. Third, particle growth during travel in lung airways is calculated. Fourth, the combined deposition efficiency of particles in each airway by various loss mechanisms is calculated. Finally, a mass balance on the traveling particles in each airway is performed, and deposition fraction per airway, generation, region, and lobe is calculated.

Since airflow travels in an airway with uniform velocity, the leading edge of the inhaled particles initially forms a front in the trachea. The front breaks up into two when reaching the first bifurcation, with each daughter front taking on a different path and continuing the transport deep into the lung until inhalation ceases. By the end of the inhalation, there will be as many fronts as the number of lung pathways traveling through the lung. With the start of the exhalation, all the fronts recede and combine when meeting at a bifurcation. Since by assumption particle transport occurs mainly by airflow convection with no axial diffusion, two daughter fronts will collapse when meeting at an airway bifurcation to form a parent front. Traveling up the airway tree, all the fronts collapse to eventually recover the original front and exit the trachea at the end of exhalation. Due to simultaneous losses of particles from the inhaled air, particle concentration in the tidal air reduces with time. The flow rates and times when the aerosol fronts cross airway proximal and distal ends are found during a breathing cycle and used to calculate particle

concentration at the proximal and distal ends of all lung airways. A mass balance on the number of inhaled particles is performed per airway to calculate airway, lobar, and regional deposition fractions.

Particles undergo growth during their transport in the lung. Airborne particles are assumed to be monodisperse. Particles enter the respiratory tract as monodisperse but change size quickly and become polydisperse. During inhalation, particles enter and exit an airway at fixed sizes since particle growth initiates at the entrance to the respiratory tract (i.e., at a constant initial diameter). The elapsed times for a particle of a given initial size to cross the proximal and distal ends of an airway are used in Equation (9) to calculate particle diameters when reaching these locations.

During the pause between inhalation and exhalation, a particle at the end of an airway grows from a size previously calculated by Equation (9) to a new size at the end of pause. Equation (9) uses the crossing time and the size of the particle at the end of inhalation as input to calculate a new size at the end of pause.

Calculations of particle growth during exhalation are more complex than those for inhalation and pause. During exhalation, the diameters of receding particles arriving at both ends of an airway vary with time since their starting locations and diameters at the beginning of exhalation are different. The largest growth is for aerosols located in the receding front since these particles have spent the greatest time in the lung. By assumption of no axial diffusion, particles in two daughter fronts that collapse into a parent front have spent the same amount of time in the lung and thus have the same diameter. Given the exhalation receding time for an aerosol front to reach the distal and proximal ends of an airway, particle diameter at these locations can be calculated from Equation (9) using, as initial condition, particle diameter in the front at the start of exhalation time.

Deposition of uncharged particles in the airways occurs by three main mechanisms—impaction, sedimentation, and diffusion (Cai and Yu 1988; Pich 1972; Ingham 1975). Each loss mechanism within an airway can be represented by a unique deposition efficiency that is defined as the fraction of entering particles that deposited in the airway. Deposition efficiency depends on particle diameter that may vary with the time that particles spend in the lung. The time an airway is occupied by particles during inhalation, pause, and exhalation was divided into N time increments, and deposition efficiency, η_i, at each time increment, Δt_i, was calculated assuming that particle size remained constant during each time increment. An average deposition efficiency, $\bar{\eta}$, was obtained during inhalation, pause, and exhalation and is given by the equation:

$$\bar{\eta} = \frac{1}{t_f - t_i}\int_{t_i}^{t_f} \eta(t)dt = \frac{1}{t_f - t_i}\sum_{i=1}^{N} \eta_i \Delta t_i$$
$$= \frac{\Delta t \sum \eta_i}{t_f - t_i} = \frac{\Delta t \sum_{i=1}^{N} \eta_i}{N\Delta t} = \frac{\sum_{i=1}^{N} \eta_i}{N}, \qquad [10]$$

where t_i and t_f are defined depending on the breathing mode. During inhalation, these times correspond to the time a front passes the proximal and distal end of an airway, respectively. During pause, t_i is the crossing time of a front at an airway end during inhalation and t_f is t_i plus pause time. During exhalation, t_i is the crossing time during inhalation plus pause time, and t_f is the time a front retreats from the airway. Particle diameters corresponding to times t_i and t_f are calculated as described previously by Equation (9), and they are used in Equation (10) to find average deposition efficiency for each loss mechanism. Losses by different mechanisms were assumed to occur independently since deposition efficiency for each mechanism was much smaller than unity in an airway. Thus the combined deposition efficiency was the sum of the average individual efficiencies.

Aerosol concentrations at the proximal and distal ends of each airway were calculated using deposition efficiencies calculated as described above. Deposited mass in each airway was computed by applying a mass balance on the particle-laden inhaled air. Particle losses were calculated at an airway size midway between lung volume at rest and maximum inhalation (that is, FRC $+V_T/2$, where V_T is the tidal volume).

RESULTS AND DISCUSSION

Particle growth in lung airways depends on particle initial diameter as well as relative humidity ($100 \times$ saturation ratio) and air temperature. While particle initial diameter can be measured, information on temperature and relative humidity in the lung is not available (Morrow 1986). This information is usually deduced by indirect measurements (Ferron et al. 1983) or numerical simulations of airflow and vapor concentration (Ferron et al. 1988a; Saranganpani and Wexler 1996). Temperature and relative humidity beyond the first few generations are found to be close to 37°C and 99.5%, respectively. In addition, growth rate varies depending on the chemical composition and concentration of the solute in the droplet. Change in the size of salt particles (NaCl with molecular weight of 58) in the lungs of human adults was calculated and compared with available data in the literature to study the growth model. Figure 1 shows the ratio of particle diameter, d_p, over its initial diameter, d_{p0}, as a function of time when placed in an environment with saturation ratios between 0.90 and 1.0. Using Equation (9), particles grew rapidly from an initial size of 0.2 μm to reach their equilibrium size in less than 1 s. The equilibrium size and time to reach this size were directly proportional to the saturation ratio. Small variations in saturation ratios above 0.98 seemed to have a significant impact on equilibrium size of the particles. Thus, it is of critical importance in experiments aimed at particle growth measurements to have good control of the saturation ratio or the ability to measure it accurately if changed during the experiment.

To evaluate the growth model, particle growth with time in a humid environment was compared against the experimental measurements of Anselm et al. (1987) for salt particles of an

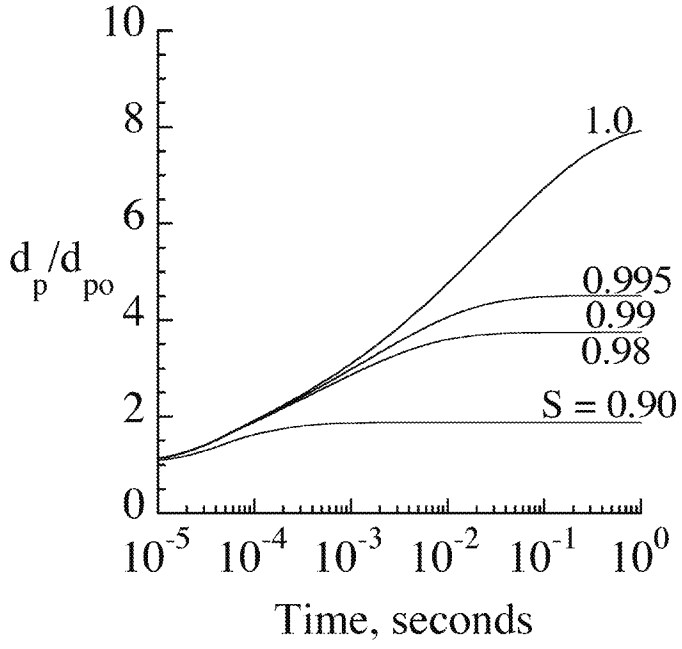

Figure 1. Predicted growth of salt particles at various saturation ratios as a function of time.

initial dry diameter of 0.7 μm. The ratios of particle diameter over its initial diameter are presented in Figure 2. There was good agreement between measurements and predictions of Equation (9) for a saturation ratio of 0.995, supporting the general consensus on relative humidity of 99.5% in the human lung (Ferron et al. 1983).

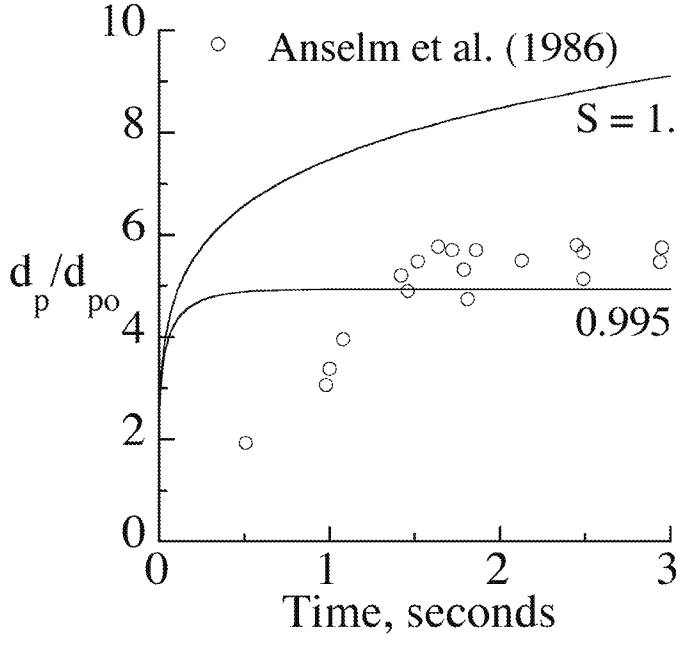

Figure 2. Calculated growth of salt particles initially at $d_{p0} = 0.7$ μm with time versus measurements.

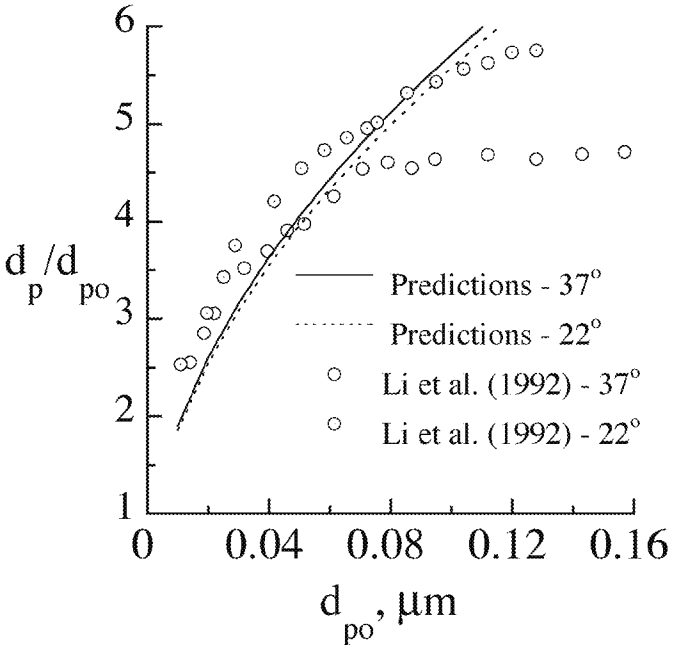

Figure 3. Comparison of the predicted and measured equilibrium diameter of salt particles in a humid environment for different initial particle sizes.

Growth of salt particles predicted by Equation (9) was further compared against experimental data of Li et al. (1992) in Figure 3. Results were calculated for particle temperatures at 37°C and 22°C, and a saturation ratio of 1. Temperature had only a minor influence on particle growth, particularly at small initial particle diameters where both predictions and measurements showed temperature independence. Our predictive model is in general agreement with the experimental measurements. Any difference between predictions and measurements is attributed to the model used to account for the solute effect (which is most accurate at a low solute concentration in the droplet) and also uncertainties surrounding relative humidity measurements throughout the experiments as discussed by Li et al. (1992).

Deposition models for hygroscopic particles are computationally more demanding than those of insoluble particles, particularly at ultrafine and submicrometer sizes. Potential prohibitive computational times impose a limitation to such calculations. The computation time is particularly large for ultrafine particles, where particle growth (Equation (9)) requires extremely small time steps for convergence. In addition, particle coagulation becomes significant for ultrafine particles since it disrupts the growth model proposed by (Equation (9)). Particle concentration in inhaled air will also be reduced, which places a limitation on applicability of the deposition model. For this reason, the computations in this article are restricted to particle diameters equal to and greater than 0.1 μm.

Use of a hygroscopic versus an insoluble model to predict deposition depends to a large degree on the extent of particle growth during its transport in the lung. The growth of salt

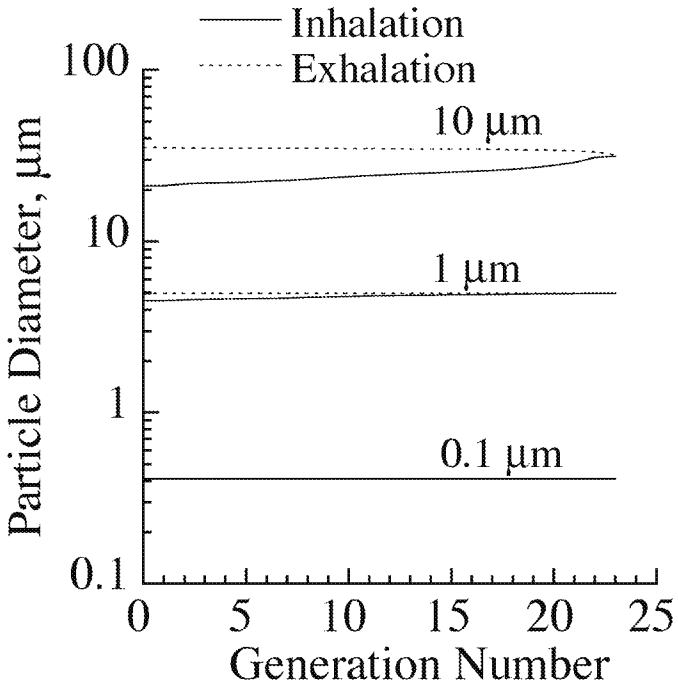

Figure 4. Growth of salt particles of different initial diameters in the respiratory tract during a single breathing cycle.

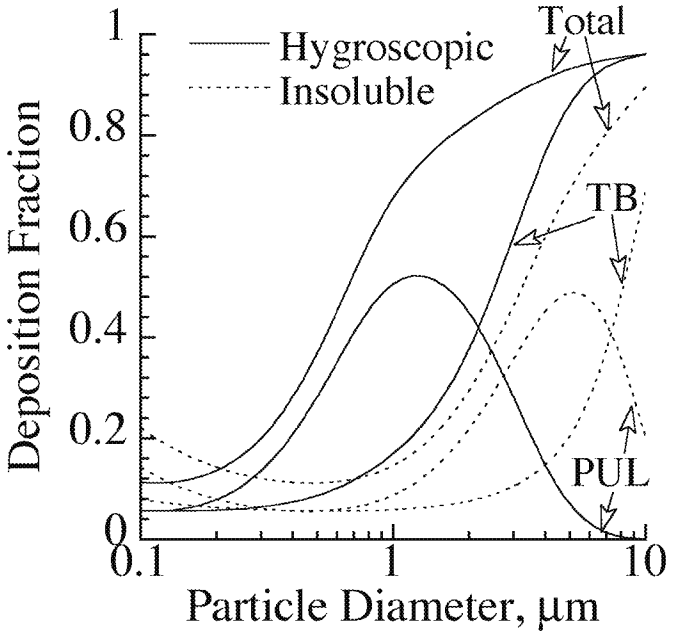

Figure 5. Regional and total deposition of hygroscopic NaCl and insoluble particles in the lung for oral breathing.

particles with initial diameters of 0.1, 1, and 10 μm was calculated in different generations of the lung during inhalation and exhalation. Results are presented in Figure 4 for a breathing period of 5 s with equal inhalation and exhalation times and zero pause time. In the model, particles travel through the head region to reach the lung. The average residence time of particles in the head region was about 0.08 s. A saturation ratio of 0.995 and temperature of 37°C throughout the respiratory tract, including the extrathoracic region, were assumed. Particles with an initial diameter of 0.1 μm grew about 4-fold to reach their equilibrium size while still in the head region. No further size change was observed in the lung. A similar growth pattern was observed for 1 μm particles. Following a nearly 4.5-fold increase in the head region, particle diameter increased slightly during inhalation, but there was no further size increase during exhalation. Particles with an initial diameter of 10 μm showed continuous growth during both inhalation and exhalation following a 2-fold diameter increase in the head section. Based on the results presented in Figure 4, the equilibrium size of submicrometer particles in a humid environment may be used in a deposition model for insoluble particles to calculate deposition of hygroscopic particles because particle growth occurs entirely before entering the lung. Inclusion of the growth model is absolutely required in the deposition calculations of hygroscopic particles with initial diameters in the fine and coarse size range.

To study the significance of various particle loss mechanisms in the lung, deposition fractions of particles in the respirable size range were calculated via oral breathing for a typical lung tidal volume of 625 ml, breathing frequency of 15 breaths per minute with zero pause time, and functional residual capacity of 3300 ml in an asymmetric human lung geometry containing approximately 32,000 conducting airways. Deposition fractions in the tracheobronchial (TB) and pulmonary (PUL) regions, and total lung are given in Figure 5 for both hygroscopic and insoluble particles. Due to particle growth, diffusion losses of submicrometer-size particles (<0.3 μm) were decreased, while impaction and sedimentation losses for fine and coarse particles were increased in the TB region. A similar trend was also observed for deposition in the PUL region despite the filtering of particles in the TB region, which created a peak in the deposition curve for fine and coarse particles. The net result was that lung deposition of hygroscopic particles was significantly larger than that of insoluble ones. The shapes of regional and lung deposition curves for hygroscopic particles were similar to the corresponding ones for insoluble particles. The curves essentially shifted to the left, reflecting the growth of particles to a larger size, which altered various particle loss mechanisms in lung airways.

The model developed in this study allows prediction of hygroscopic particle deposition in symmetric as well as nonsymmetric airway geometry models. Most of the available models in the literature are based on a symmetric lung structure (e.g., Weibel 1963; Yeh and Schum 1980) and are unable to predict variation of dose in the lung airways due to asymmetric nature of the lung geometry. This effect, although insignificant when interested in regional deposition predictions of insoluble particles (Asgharian et al. 2001), may become significant for the case of hygroscopic particles since particle growth depends on travel time of particles in the lung and is thus pathway-dependent. In

addition, particle growth is nonlinear (Equation (9)), while airway dimensions in a symmetric geometry model are algebraic averages of the measured dimensions in various pathways. To investigate the significance of including the details of the geometry, a comparison of deposition of hygroscopic and insoluble particles in symmetric and asymmetric lung structures was made in Figures 6a–c for the case of nasal breathing at a tidal volume of 625 cm^3 and breathing frequency of 15 breaths per minute. Deposition calculations were made for particle diameters between 0.1 μm and 10 μm. The comparison in the TB region is shown in Figure 6a. Particle deposition was higher in symmetric lung geometries for hygroscopic and insoluble particles. In addition, the shapes of the deposition curves were similar for both particle types. Similar trends were observed in the PUL region (Figure 6b) and the entire respiratory tract (Figure 6c). In essence, the difference in the magnitude of deposition of

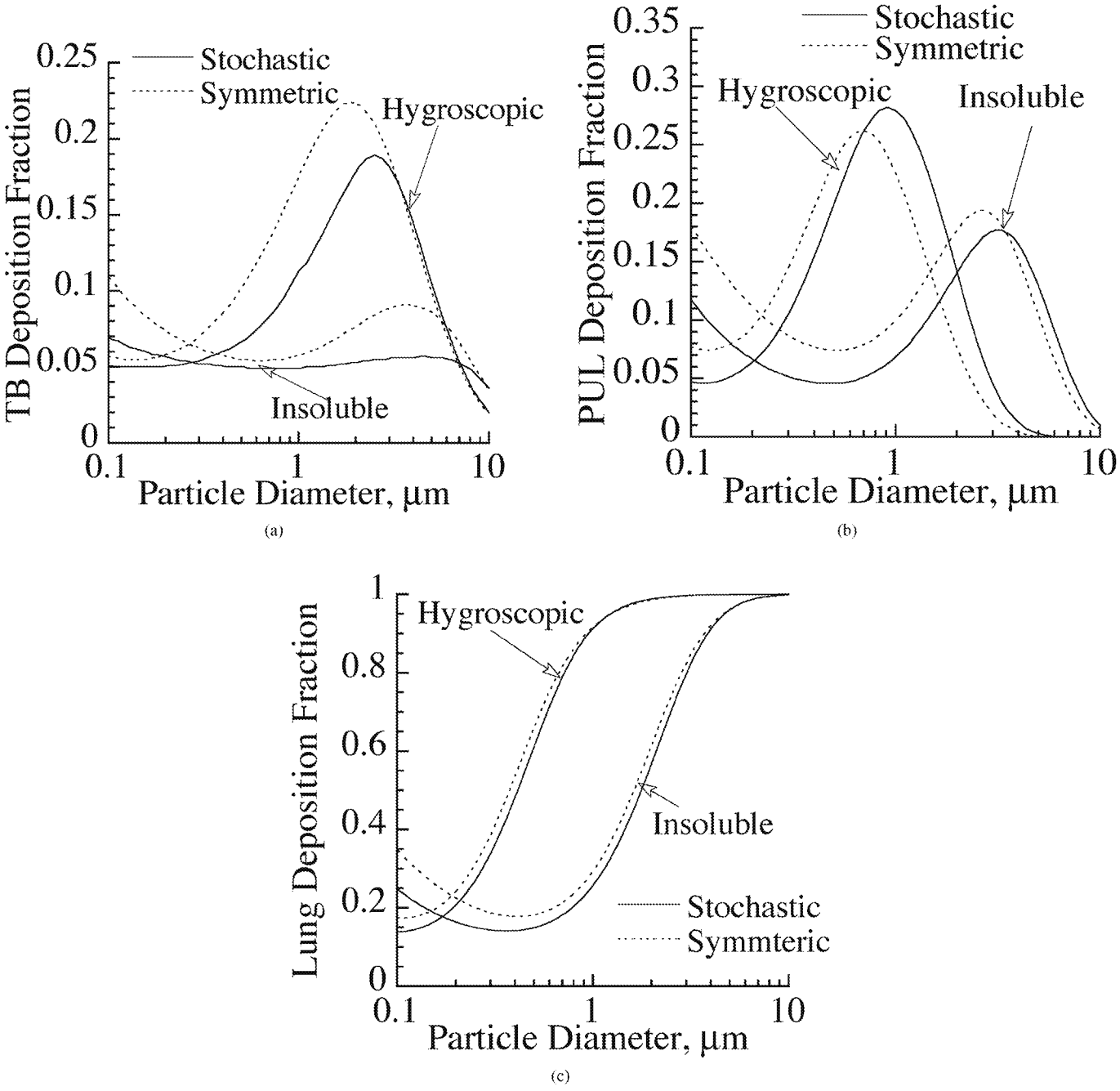

Figure 6. Deposition of hygroscopic NaCl and insoluble particles in symmetric and stochastic lung geometries for (a) tracheobronchial deposition, (b) pulmonary deposition, and (c) total deposition. Breathing route is through nasal passages.

insoluble particles between symmetric and asymmetric lung geometries was retained for hygroscopic particles as well. This difference was noticeable for regional deposition (TB and PUL) but fairly small for total deposition. Although not shown, the difference in deposition between symmetric and asymmetric lung structures became even greater when deposition per generation or site-specific deposition was studied. Detailed morphometry of the lung exerted a strong, dominant influence on localized deposition of particles in the lung. Based on the results in Figure 6, the asymmetric lung model should be used when interested in regional deposition, but the symmetric lung geometry may be used to calculate total lung deposition in order to save computation time.

To study deposition distribution of hygroscopic versus insoluble particles in the lung, deposition fractions of 0.1, 1, and 10 μm particles were calculated in various generations of the lung via nasal breathing for a tidal volume of 625 cm^3 and breathing frequency of 15 breaths per minute. The results are presented in Figures 7a–c. The results for 0.1 μm particles are shown in Figure 7a. There was a small deposition in the upper airways

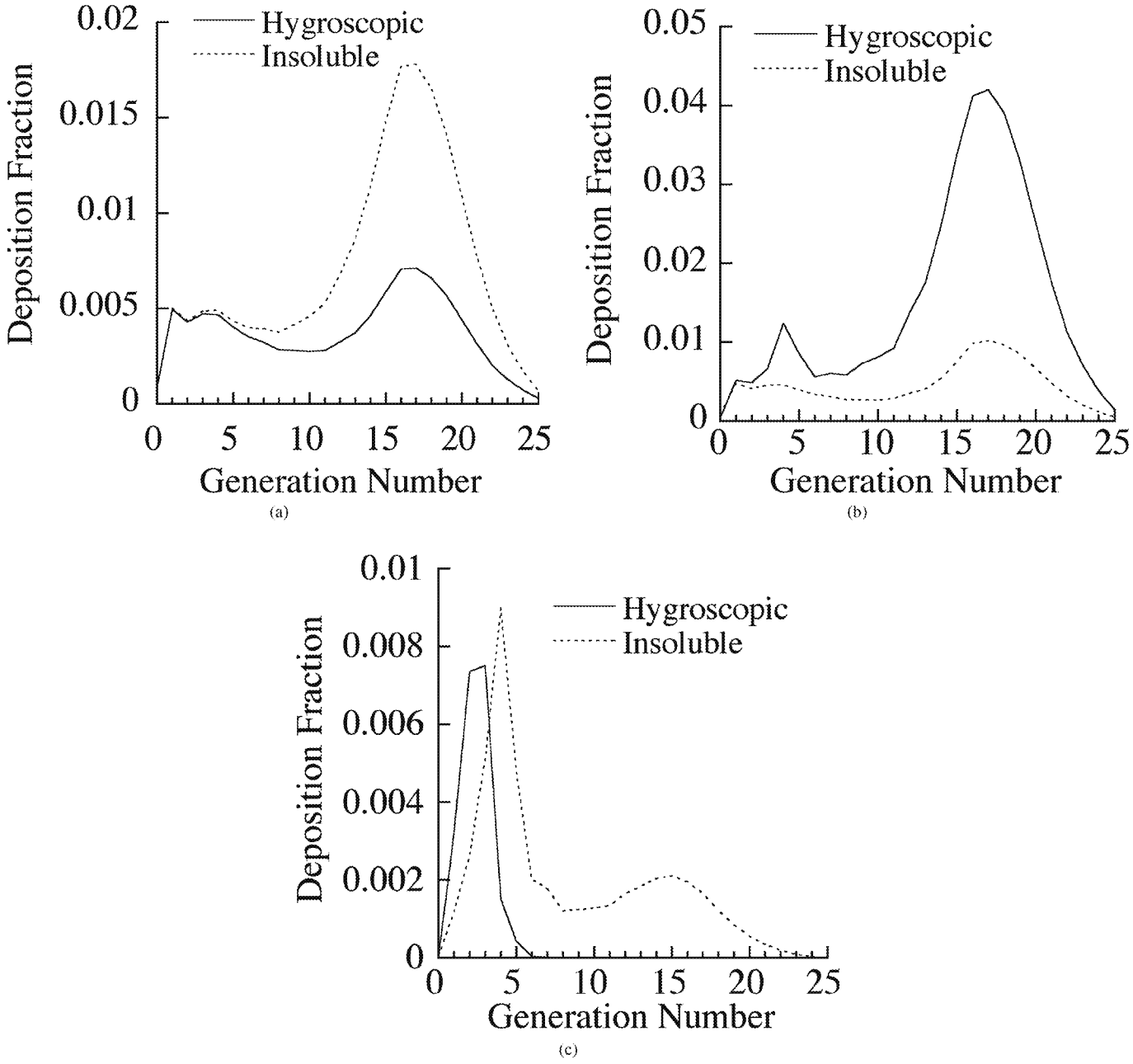

Figure 7. Deposition fraction of hygroscopic NaCl and insoluble particles in various generations of a stochastic lung for particle diameter (a) 0.1 μm, (b) 1 μm, and (c) 10 μm.

and a significant deposition in the deep lung (PUL region or airway generations 16 and higher) by diffusion for insoluble particles. Hygroscopic particles with an initial diameter of 0.01 μm grew in the head region to about 0.4 μm and entered the lung. Consequently, there was a significant reduction in deposition as compared with that of insoluble particles because submicron particles deposited predominantly by diffusion, which decreased with particle size.

Particle growth produced an opposite effect on the deposition of 1 μm particles (Figure 7b). Minimal lung deposition occurred for insoluble 1 μm diameter particles. A slight increase in deposition by impaction occurred in the upper airways of the TB region, but there was a significant increase in the deposition of 1 μm initial size hygroscopic particles in the lower airways (generations 16 and higher) of the lung due to enhanced sedimentation losses. For 10 μm particles (Figure 7c), most of the deposition occurred in the upper airways of the TB region by impaction for both hygroscopic and insoluble particles. There was also some deposition of insoluble particles in the lower airways of the lung by sedimentation. An interesting observation to note was the lack of any deposition of hygroscopic particles in the deep lung, because all the inhaled particles had already deposited in the head and TB regions.

In recent years, the delivery of therapeutic aerosols to the lung has received increasing attention in the pharmaceutical industry. Inspection of Figures 7a–c offers a guideline for the delivery of hygroscopic aerosols to the lung. Based on Figure 7c, coarse aerosol drugs should be used for targeting upper airways of the lung. On the other hand, fine-size particles are ideal for deep lung delivery (Figure 7b). Submicron sizes may be used for targeting the entire lung, but a high concentration of the aerosols in the exposure atmosphere is required since the deposition fraction of submicrometer particles is small (Figure 7a). Alternatively, a combination of fine and coarse particles can be used for lung delivery if nasal delivery of the drug particles is also desired. It should be noted that the findings based on Figure 7 are only applicable to particles with physicochemical properties similar to that of salt particles. The proposed model can be run for other types of hygroscopic drug aerosols to formulate an appropriate delivery regimen. The results in Figure 7 will also change for oral or endotracheal breathing.

Lastly, the deposition model presented in this article was tested by comparing the predicted values against data available in the literature (Tu and Knudson 1984) using corresponding breathing and lung parameters. Identical particle sizes and chemical composition were also used for comparison of the predictions against the measurements. The measured deposition fractions of two studies are plotted against model predictions at the same conditions in Figure 8. Also included in Figure 8 is the line of identity, indicating when there is a perfect match between measurements and predictions. The calculated points in Figure 8 clustered around the line of identity at small deposition fractions and are both above and below the line, indicating that (1) the agreement is satisfactory and (2) there is no bias toward

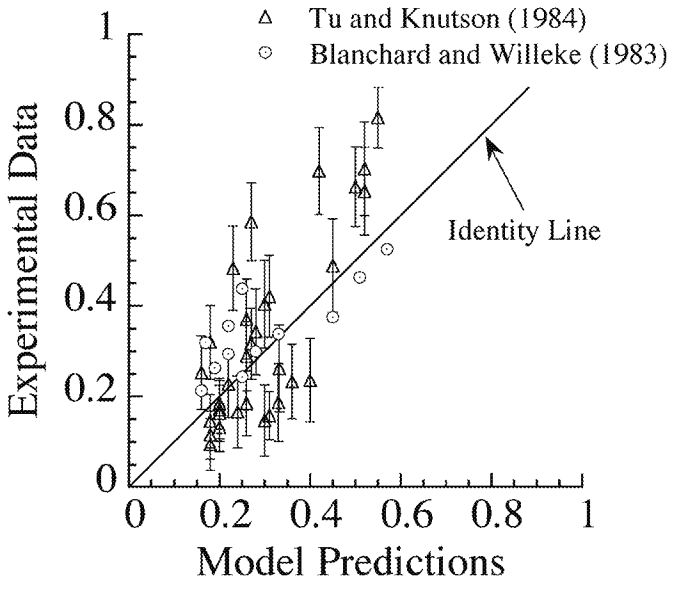

Figure 8. Comparison of predicted deposition fraction of hygroscopic NaCl particles in the lung to experimental measurements.

overprediction or underprediction. However, a few points, particularly at large deposition fractions, were clearly away from the identity line, indicating a weak correlation between predictions and reported data. This could be due to variability in lung geometries or breathing parameters.

SUMMARY

A mathematical model for the deposition of hygroscopic particles in asymmetric lung geometries of humans was developed. Particle growth was the result of molecular diffusion of water vapor in the air to the surface of the particles. The growth model included Kelvin, Fuchs, temperature depression, and solute effects. The growth calculated for salt particles agreed with available measurements in the literature. Particles of 0.2 μm initial diameter reached their equilibrium size in less than 1 s. Time to reach equilibrium size was proportional to initial size of the particles. It was found that submicron particles behave essentially as insoluble in the lung since they have attained their equilibrium size when entering the lung.

Particle growth reduced diffusive losses and increased sedimentation and impaction losses in the lung. The model was able to calculate deposition of hygroscopic particles in symmetric and asymmetric lung geometries. Morphometrically based, realistic lung geometries are crucial for accurate calculation of site-specific and regional deposition of particles in the lung. For lung deposition (TB plus PUL), however, symmetric geometries give a reasonable prediction of deposition and thus are recommended when reduction in computation time is desired. Particle hygroscopicity can be exploited for optimal drug delivery to the lung. Coarse drug particles are recommended for targeting the

upper airways in the TB region. Fine aerosol drugs, on the other hand, are ideal for delivery to the pulmonary region. Submicron particles or a combination of fine and coarse aerosols can be employed for targeting the entire lung.

REFERENCES

Anjilvel, S., and Asgharian, B. (1995). A Multiple Path Model of Particle Deposition in the Rat Lung, *Fundam. Appl. Toxicol.* 28:41–50.

Anselm, A., Gebhart, J., Heyder, J., and Ferron, G. (1987). In *Aerosols: Formation and Reactivity*, Pergamon Press, Oxford, pp. 252–255.

Asgharian, B., Hofmann, W., and Bergmann, R. (2001). Particle Deposition in a Multiple-Path Model of the Human Lung, *Aerosol Sci. Technol.* 34:332–339.

Broday, D. M., and Georgopoulos, P. G. (2001). Growth and Deposition of Hygroscopic Particulate Matter in the Human Lung, *Aerosol Sci. Technol.* 34:144–159.

Cai, F. S., and Yu, C. P. (1988). Inertial and Interceptional Deposition of Spherical Particles and Fibers in a Bifurcating Airway, *J. Aerosol Sci.* 19:679–688.

Davies, C. N. (1978). Evaporation of Airborne Droplets. In *Fundamentals of Aerosol Science*, edited by D. T. Shaw. Wiley, New York.

Ferron, G. A., Haider, B., and Kreyling, W. G. (1983). The Size of Soluble Aerosol Particles as a Function of the Humidity of the Air. Application to the Human Respiratory Tract, *J. Aerosol Sci.* 3:196–201.

Ferron, G. A., Haider, B., and Kreyling, W. G. (1988a). Inhalation of Salt Aerosol Particles I. Estimating of the Temperature and Relative Humidity of the Air in the Human Upper Airways, *J. Aerosol Sci.* 19(3):343–363.

Ferron, G. A., Kreyling, W. G., and Haider, B. (1988b). Inhalation of Salt Aerosol Particles II. Growth and Deposition in the Human Respiratory Tract, *J. Aerosol Sci.* 19(5):611–631.

Friedlander, S. K. (1977). *Smoke, Dust, and Haze, Fundemental of Aerosol Behavior*. John Wiley & Sons Inc., New York, p. 222.

Hinds, W. C. (1999). *Aerosol Technology*. John Wiley & Sons Inc., New York, p. 253.

Ingham, D. B. (1975). Diffusion of Aerosols from a Stream Flowing through a Cylindrical Tube, *J. Aerosol Sci.* 6:125–132.

Li, W., Montassier, N., and Hopke, P. K. (1992). A System to Measure the Hygroscopicity of Aerosol Particles, *Aerosol Sci. Technol.* 17:25–35.

Lippmann, M., and Thurston, G. D. (1996). Sulfate Concentrations as an Indicator of Ambient Particulate Matter Air Pollutant for Health Risk Evaluations, *J. Expo. Anal. Environ. Epidemiol.* 6(2):123–146.

Martonen, T. B. (1982). Analytical Model of Hygroscopic Particle Behavior in Human Airways, *Bull. Math. Biolog.* 44(3):425–442.

Martonen, T. B., and Zhang, Z. (1993). Deposition of Sulfate Acid Aerosols in the Developing Human Lung, *Inhal. Toxicol.* 5:165–187.

Morrow, P. E. (1986). Factors Determining Hygroscopic Aerosol Deposition in Airways, *Physiol. Rev.* 66(2):330–376.

Persons, D. D., Hess, D., Muller, W. J., and Scherer, P. W. (1987). Airway Deposition of Hygroscopic Heterodispersed Aerosols: Results of a Computer Calculation, *J. Appl. Physiol.* 63(3):1195–1204.

Pich, J. (1972). Theory of Gravitational Deposition of Particles from Laminar Flows in Channels, *J. Aerosol Sci.* 3:351–361.

Robinson, R. J., and Yu, C. P. (1998). Theoretical Analysis of Hygroscopic Growth Rate of Mainstream and Sidestream Cigarette Smoke Particles in the Human Respiratory Tract, *Aerosol Sci. Technol.* 28:21–32.

Sarangapani, R., and Wexler, A. S. (1996). Growth and Neutralization of Sulfate Aerosols in Human Airways, *J. Appl. Physiol.* 81(1):480–490.

Spengler, J. D., Brauer, M., amd Koutrakis, P. (1990). Acid Air and Health, *Environ. Sci. Technol.* 24:946–956.

Spurny, K. R. (1996). Chemical Mixtures in Atmospheric Aerosols and Their Correlation to Lung Diseases and Lung Cancer Occurrence in the General Population, *Toxicol. Lett.* 88:271–277.

Stapleton, K. W., Finlay, W. H., and Zuberbuhler, P. (1994). An in vitro Method for Determining Regional Dosage Delivered by Jet Nebulizers, *J. Aerosol Med.* 7:325–344.

Thurston, G. D., Ito, K., Hayes, C. G., Bates, D. V., and Lippmann, M. (1994). Respiratory Hospital Admissions and Summertime Haze Air Pollution in Toranto, Ontario: Consideration of the Role of Acid Aerosols, *Environ. Res.* 65:271–290.

Tu, K. W., and Knutson, E. O. (1984). Total Deposition of Ultrafine Hydrophobic and Hygroscopic Aerosols in the Human Respiratory System, *Aerosol Sci. Technol.* 3:453–465.

U.S. Environmental Protection Agency (USEPA). (1996). *Air Quality Criteria for Particulate Matter*. Report no. EPA/600/P-95/001aF, US Environmental Protection Agency, Research Triangle Park, NC.

Van Wylen, G. J., and Sonntag, R. E. (1973). *Fundamentals of Classical Thermodynamics*. John Wiley and Sons, Inc., New York, p. 367.

Weibel, E. R. (1963). *Morphometry of the Human Lung*. Academic Press, New York.

Xu, G. B., and Yu, C. P. (1985). Theoretical Lung Deposition of Hygroscopic NaCl Aerosols, *Aerosol Sci. Technol.* 4:445–461.

Yeh, H., and Schum, G. M. (1980). Models of Human Lung Airways and Their Application to Inhaled Particle Deposition, *Bull. Math. Biol.* 42:461–480.

Yu, C. P. (1978). Exact Analysis of Aerosol Deposition During Steady Breathing, *Powder Technol.* 21:55–62.